

Strength Evaluation of Polycrystalline Silicon Structure Considering Sidewall Morphology

S. Hamada¹, Y. Sugimoto¹
¹*Kyushu University, Fukuoka, Japan*

Abstract

In order to evaluate strength of micron size polycrystalline silicon (poly-Si) structure for MEMS considering surface morphology difference between top and sidewall and effective surface area, bending strength tests of cantilever beam, surface roughness measurement and fracture surface analysis are performed. The specimens are made by CVD process for poly-Si deposition and deep RIE process for sidewall formation, and then the surface morphology of the top and the sidewall surface are different. The various size notches on the specimen are introduced in order to change effective surface area. By the fracture surface analysis, it was found that the fracture initiation point was not always maximum stress point; this is because there exist stress concentration on the surface. Surface roughness was measured using atomic force microscope (AFM). Then the maximum stress concentration of the specimen on the top and the sidewall surface respectively were presumed using extreme statistics, and effective surface area was defined. Then, bending strength and effective surface area shows good correlation.

Key words: Poly-Si, MEMS, Bending strength, Stress concentration, Size effect, Scallop

1. Introduction

Polycrystalline silicon (poly-Si) structure is widely employed in the Micro-Electro-Mechanical Systems (MEMS) [1,2]. MEMS devices, which contain mechanical movement, have to maintain their reliability in face of external shock, thermal stress and residual stress from manufacturing processes, and fracture will begin mainly in stress concentration area. Therefore, it is necessary to build up reliability design criterion of the poly-Si structure that has stress concentration [3-9]. However, since the size effect is large, the microscopic poly-Si depends for the strength on the effective area caused by the stress concentration of structure. Moreover, as the point peculiar to the microscopic poly-Si at the time of thinking of strength, in order that the techniques of processing the upper surface and the sidewall surface differ, it is mentioned that the surface roughness used as the source of a stress concentration differs. It depends for the strength of the microscopic poly-Si also on surface roughness. Therefore, it is necessary to deal with simultaneously the stress concentration of structure and the stress concentration by surface roughness in the case of strength evaluation. In order to clarify the bending strength and its effective area dependability of poly-Si, bending tests using micro scale cantilever beams with or without notch of several

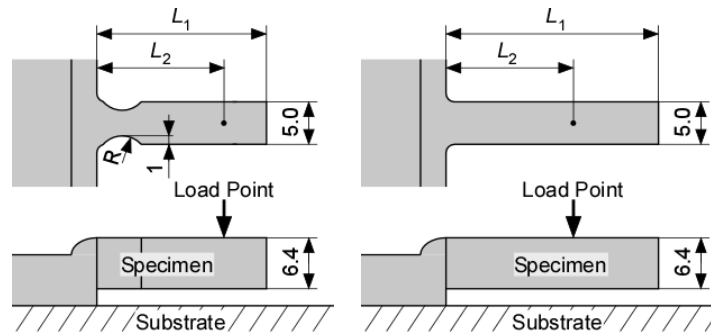
sizes are performed. Moreover, surface roughness measurement using AFM is carried out, it determines for the stress concentration by surface roughness, and a quantitative effective area is defined. Fracture origins are specified by fracture surface observation, and the validity of the effective area are shown. Finally, the static strength design criteria in consideration of scattering in strength which used two parameters, the maximum stress and an effective area, are proposed.

2. Test Method

2.1 Specimen

The specimens are illustrated in Fig. 1. Shapes and dimensions of the specimens are shown in Table 1. For bending tests, two types of specimens; Type-A and B are prepared. In the Type-A specimen, the notch of several sizes (1~5 [μm]) is introduced in the root section of micro-cantilever beam. In the Type-B, by the microscopic observation, the 1 [μm] corner radius is recognized indeed in the root section of micro cantilever beam. Thickness of the specimen is 6.4 [μm].

The poly-Si is chemical vapor deposited (CVD) on single crystal silicon wafer surface, and the specimens are made from surface micromachining process. The gap between the cantilever and the substrate is 2 [μm]. The Deep Reactive Ion Etching (DRIE) process was used for processing of the sidewall surface. Therefore, in the specimen side surface, microscopic irregularity called “scarop” which is not seen on the upper surface. Figure 2 shows the example of the scarop.



(a) Notched specimen (Type-A) (b) Specimen without notch (Type-B).

Fig. 1 Schematic diagram of the specimens (unit: μm)

Table 1 Shapes and dimensions of the specimen

| Specimen Type | L_1 , μm | L_2 , μm | R , μm |
|---------------|-----------------------|-----------------------|---------------------|
| Type-A L15R1 | 20 | 15 | 1 |
| L15R2 | 20 | 15 | 2 |
| L15R3 | 20 | 15 | 3 |
| L15R4 | 20 | 15 | 4 |
| L15R5 | 20 | 15 | 5 |
| Type-B L10 | 15 | 10 | – |
| L15 | 25 | 15 | – |

2.2 Strength test and stress analysis

A dynamic ultra micro hardness tester (Shimadzu DUH-W201) with a Berkovich diamond indenter is used for the bending tests. The test machine is for hardness test but we can obtain the relationship between load and displacement with satisfactory accuracy by this machine. The test load speed is 1.421 [mN/sec.]. The bending tests are carried out at room temperature under the atmospheric environment. Figure 3 shows examples of the relationship between load and displacement of the bending tests. In this figure, the poly-Si deformed elastically until final catastrophic failure, showing a brittle nature.

In order to quantify the fracture of specimens by the applied stresses in the tests, three-dimensional finite element elastic analyses using commercial FEM solver ANYSS 10.0 are performed.

2.3 Surface roughness

In order to investigate the stress concentration by the shape of the microscopic surface of a specimen, surface shapes were measured using the atomic force microscope (AFM) (VEECO D-3000). The region to measure was made into 1 [μm] four quarters. The upper surfaces were measured by scanning in the specimen longitudinal direction, and the sidewall surface scanned and measured the scarop bottom in the specimen longitudinal direction. The maximum stress concentration factor $K_{t \max}$ which exists in a specimen was determined using the roughness of the measured surface. It is shown in 4.1 for details. In order to estimate the maximum stress concentration factor which exists in a specimen, the data of stress concentration factor determined by measurement was arranged using statistics of extreme [10].

2.4 Effective area

The following equations thought to be able to define an effective area S . Maximum stress σ_{\max} of the structure calculated in FEM analysis and $K_{t \max}$ calculated by roughness measurement are used. When the stress concentration

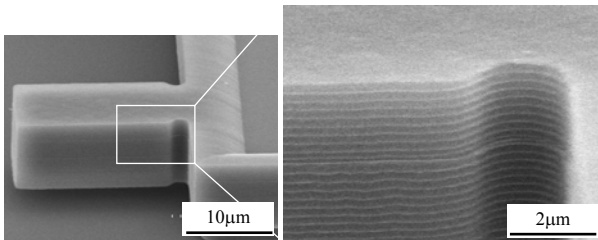


Fig. 2 Sidewall surface morphology of the poly-Si specimen.

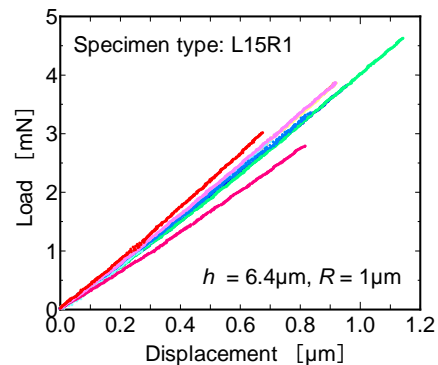


Fig. 3 Example of relationship between load and displacement.

shown in the Eq. (1) was taken into consideration, area on which the stress exceeding σ_{\max} was made into the effective area.

$$\sigma_{\max} \leq K_{t \max} \sigma \quad (1)$$

The S thought to expresses the effective area at the time of evaluating strength here. Within the range of an effective area, it can become fracture origin except the maximum stress working point by the stress concentration of structure by the surface roughness stress concentration.

3. Bending test results

In order to investigate the scattering in the fracture strength obtained by a bending strength test and FEM analysis, fracture strength was plotted to Weibull probability paper [11]. Weibull distribution is used for strength evaluation of a brittle material like the ceramics, and it is thought that Weibull distribution can estimate the strength of the poly-Si which is brittle material. The function of two population parameters Weibull distribution can be expressed with the following equation.

$$F = 1 - \exp \left\{ - \left(\frac{\sigma_B}{\sigma_0} \right)^m \right\} \quad (2)$$

In Eq. (2), F : Cumulative probability of failure, σ_0 : scale parameter, m : shape parameter, respectively. The obtained Weibull probability paper is shown in Fig. 5, and the scale parameter of each specimen shape are shown in Fig. 6. Figure 6 shows that a scale parameter indicates the tendency which becomes small as the notch radius R becomes large. It is possible that this is because the effective area on the surface of a specimen increased.

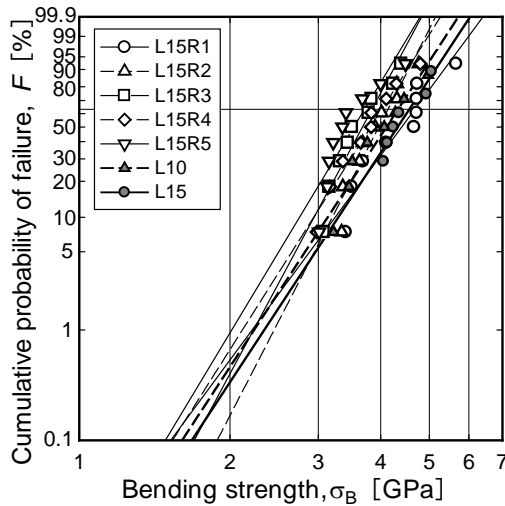


Fig. 5 Weibull plots of bending strength for poly-Si

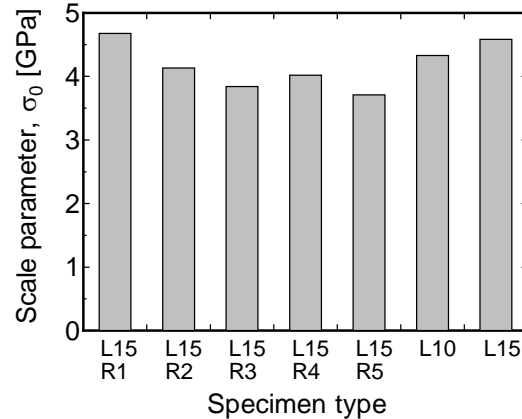


Fig. 6 Scale parameter of bending strength for poly-Si

4. Effective area and application to design

4.1 Effective area definition and calculation results

The stress concentration factors on the specimen surface were determined based on the result of surface roughness measurement by AFM. As shown in Fig. 2, difference occurs in the surface shape of the upper surface and the sidewall surface by the difference in the manufacturing technique. Figure 7 indicates an example of the difference in surface roughness obtained by AFM, and Fig. 8 indicates the example of surface section of the scarop bottom on the sidewall surface.

Using the measurement result of the surface roughness, the stress concentration factors K_t of the specimen were calculated. As shown in Fig.7, the appearance present complicated shapes, therefore FEM analysis is necessary to calculate an accurate stress concentration factors. In this report, in order to simplify, the interference effects by the multiple notches were ignored and the stress concentration factors K_t were determined from width (a) and depth (b) from the roughness measurements using the following equations supposing the equivalent ellipse as shown in Fig.8.

$$K_t = 1 + \frac{2a}{b} \quad (3)$$

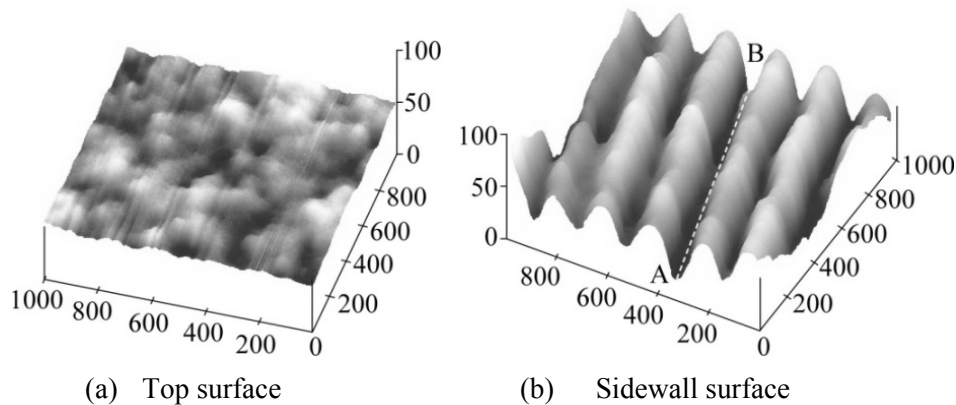


Fig. 7 Surface morphology of top and sidewall (unit: nm).

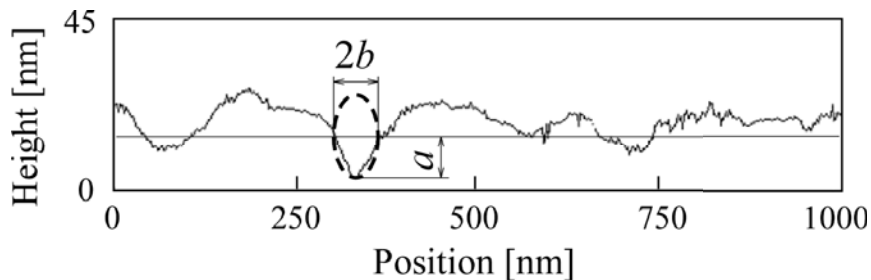


Fig. 8 Surface roughness example of sidewall (Fig. 7 A-B)

The maximum stress concentration factor $K_{t \max}$ which exists in a specimen based on the data of the measured stress concentration factor is estimated using the statistics of extreme. Figure 9 shows the extreme values probability paper. The horizontal axis is the stress concentration factor K_{tj} obtained by the Eq. (3). The vertical axis is the reduced variates y_j calculated by the following equation which is a formula of the statistics of extreme.

$$F_j = \frac{j}{n+1}, \quad y_j = -\ln\{-\ln F_j\} \quad (4)$$

$(j = 1, 2, 3, \dots, n \quad n: \text{Number of inspections})$

The approximate expression was calculated using the least square method from the obtained distribution. The maximum stress concentration factor which substitutes the return period T for the following equations, and $K_{t \max}$ exist in a specimen is estimated.

$$y = -\ln\left\{-\ln\left(\frac{T-1}{T}\right)\right\}, \quad y = \alpha K_{t \max} + \beta \quad (5)$$

When determining the return period T , evaluation area was made equal to the effective area. The relation between evaluation area and the return period are defined using the following equations. (S_0 : inspection area)

$$T_i = \frac{S_i + S_0}{S_0}, \quad S < 10 S_0 \quad (6)$$

$$T_i = \frac{S_i}{S_0}, \quad S > 10 S_0 \quad (7)$$

In order to bring evaluation area close to an effective area, calculation performed repeatedly. The computational procedure is as follows. Fig. 10 indicates a computational procedure outline.

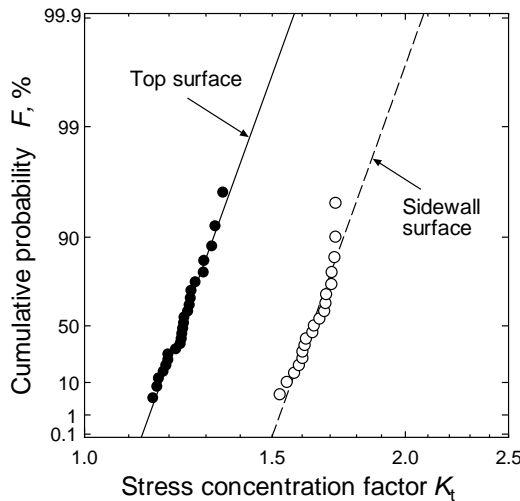


Fig. 9 Variation of stress concentration factor K_t

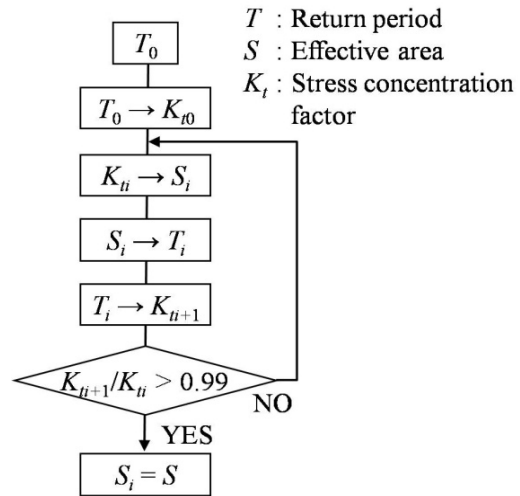


Fig. 10 Schematic diagram of deciding S from T and K_t .

- 1) Define T_0 by the evaluation area to the extent of the whole specimen is included enough
- 2) Calculate K_{t_i} from defined T_0
- 3) Calculate assumed effective area S_i from Eq. (1) and FEM
- 4) Calculate T_i, S_i as evaluation area
- 5) Calculate $K_{t_{i+1}}$ from T_i
- 6) Compare K_{t_i} and $K_{t_{i+1}}$. If $K_{t_i}/(K_{t_{i+1}}) > 0.99$, then define S_i as effective area
- 7) If not $K_{t_i}/(K_{t_{i+1}}) > 0.99$, repeat the process after 3).

In this study, it calculated as initial return period value $T_0 = 10000$. Table 2 shows the obtained $K_{t_{\max}}$ and S .

4.2 Effective area and fracture origin

Figure 11 indicates the example in the structure of the effective area. Figure 11 shows that the region of effective area where fracture origin may exist has extended to the specimen sidewall. Fracture surface observation of the specimen was carried out, and the example to which fracture origin exists in the sidewall was observed. Figure 12 shows an example. The scattering in fracture origin is shown in Fig. 13. It turns out that fracture origin varies within an effective area.

Table 2 Result of calculations, $K_{t_{\max}}$ and S

| Specimen type | Maximum stress concentration factor | | Effective area $S [\mu\text{m}^2]$ |
|---------------|-------------------------------------|------------------|---------------------------------------|
| | Top surface | Sidewall surface | |
| L15R1 | 1.22 | 1.79 | 4.02 |
| L15R2 | 1.28 | 1.82 | 8.01 |
| L15R3 | 1.34 | 1.84 | 13.7 |
| L15R4 | 1.39 | 1.86 | 22.7 |
| L15R5 | 1.39 | 1.85 | 22.8 |
| L10 | 1.20 | 1.78 | 3.57 |
| L15 | 1.21 | 1.78 | 3.47 |

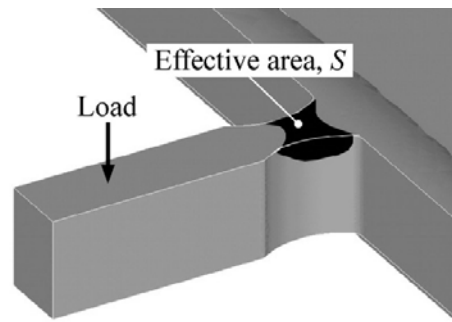


Fig. 11 Calculated effective area S (Specimen type: L15R5).

4.3 Application to design

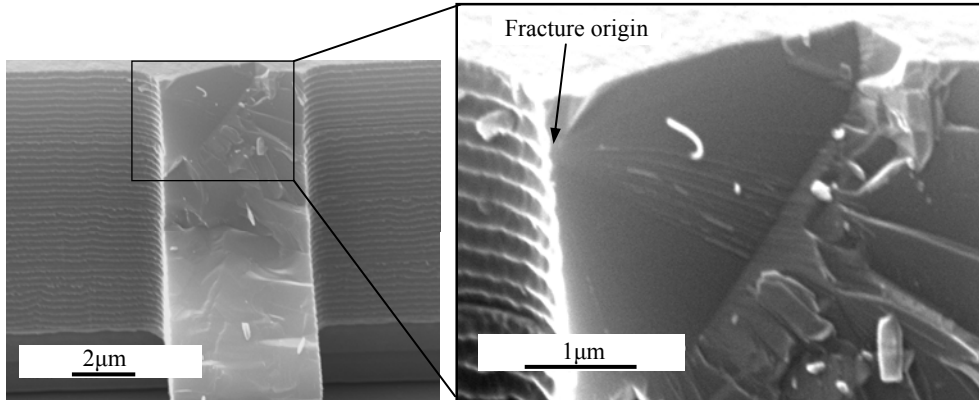
Bending strength (maximum stress σ_{\max} at the time of fracture) σ_B and the maximum stress concentration factor $K_{t \max}$ were fitted to the Eq. (1) and the effective area was determined. Figure 14 shows the relationship between bending strength and the effective area. Average values of the test data ($N = 8$) were used for σ_B . The tendency bending strength becomes small as the effective area increased can be seen.

The equation of Weibull distribution which generally took the effective volume V into consideration is shown as follows.

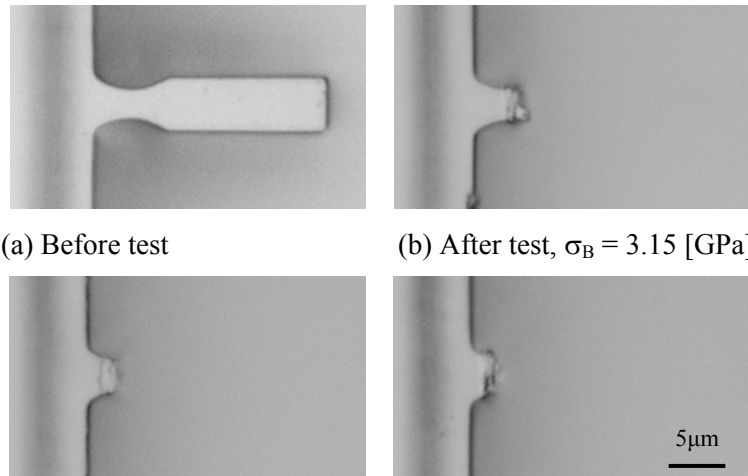
$$F = 1 - \exp \left\{ -V \left(\frac{\sigma_B}{\sigma_0} \right)^m \right\} \quad (8)$$

Eq. (8) can be expressed as follows.

$$\ln \ln \frac{1}{1-F} = m(\ln \sigma_0 - \ln \sigma_B) + \ln V \quad (9)$$



(a) Whole fracture surface (b) Magnification of fracture origin
Fig. 12 Fracture origin on the sidewall surface.



(a) Before test (b) After test, $\sigma_B = 3.15$ [GPa]
(c) After test, $\sigma_B = 3.41$ [GPa] (d) After test, $\sigma_B = 3.67$ [GPa]
Fig. 13 Variation of fracture points, Specimen type: L15R5.

It turns out in the Eq. (9) that the effective volume V acts as a value which does not involve at the shape parameter m which shows the level of scattering. Since an effective volume did not participate in scattering, it extrapolated to the reliability needed for a design using the average of the shape parameter determined from the experimental result σ_B . In Fig. 14, an extrapolation example in the case of $F = 0.001$, the relationship between σ_B and S are shown.

5. Conclusion

In order to propose the static strength design criteria of the poly-Si structure which has a microscopic dimension, the bending test, surface roughness measurement, FEM analysis, the Weibull statistical analysis, statistics of extreme analysis, and fracture analysis of a cantilever beam were conducted.

The obtained results are as follows.

- (1) The definition method of the quantitative effective area in bending cantilever beam was shown to the poly-Si with which the surface roughness on the upper surface and the surface of the sidewall differs.
- (2) Bending strength depends on the effective area definition are shown.
- (3) The static strength design criteria in consideration of the scattering in the strength using two parameters, the bending strength (maximum stress at the time of fracture) and the effective area, was proposed.

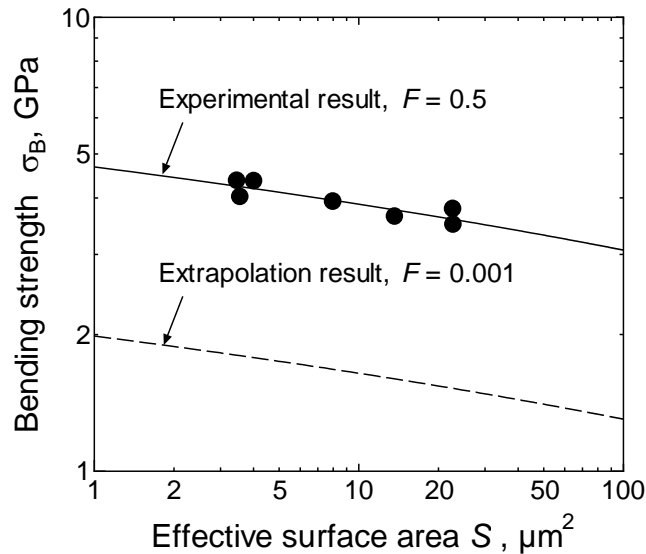


Fig. 14 Relationship between the bending strength and effective area

Reference

- [1] S. D. Senturia, *Microsystem Design*, Kluwer Academic Publishers, Dordrecht, 2000
- [2] K. Najafi, *Micromachined Micro Systems: Miniaturization Beyond Microelectronics*, Proc. 2000 Symposium on VLSI Circuits Digest of Technical Papers (2000) 6-13
- [3] S. Greek, F. Ericson, S. Johansson and J.-Å. Schweitz, In situ tensile strength measurement and Weibull analysis of thick film and thin film micromachined polysilicon structures, *Thin Solid Films* 292 (1997) 247-254
- [4] T. Tsuchiya, O. Tabata, J. Sakata and Y. Taga, Specimen size effect on tensile strength of surface micromachined polycrystalline silicon thin films, *IEEE J. Microelectromechanical Systems* 7 (1998) 106-113
- [5] T. Namazu, Y. Isono and T. Tanaka, Evaluation of Size Effect on Mechanical Properties of Single Crystal Silicon by Nano-Scale Bending Test using AFM, *IEEE J. Microelectromechanical Systems* 9 (2000) 450-459
- [6] H. Kapels, R. Aigner and J. Binder, Fracture strength and fatigue of polysilicon determined by a novel thermal actuator, *IEEE Trans. Electron Devices*, 47 (2000) 1522-1528
- [7] W. N. Sharpe Jr., K. M. Jackson, K. J. Hemker and Z. Xie, Effect of Specimen Size on Young's Modulus and Fracture Strength of Polysilicon, *IEEE J. Microelectromechanical Systems* 10 (2001) 317-326
- [8] K. S. Chen, A. A. Ayón, X. Zhang and S. M. Spearing, Effect of Process Parameters on the Surface Morphology and Mechanical Performance of Silicon Structures After Deep Reactive Ion Etching (DRIE), *IEEE J. Microelectromechanical Systems* 11 (3) (2002) 264-275
- [9] C. L. Muhlstein, R. T. Howe and R. O. Ritchie, Fatigue of Polycrystalline Silicon for Microelectromechanical Systems: Crack Growth and Stability under Resonant Loading Conditions, *Mechanics of Materials* 36 (2004) 13-33
- [10] E. J. Gumbel, *Statistic of Extremes*, Columbia Univ. Press, New York, 1962
- [11] W. Weibull, A statistical distribution function of wide applicability, *Trans. ASME J. Appl. Mech.* 18 (1951) 293-297